ARTICLE OPEN

Check for updates

On the accurate characterization of quantum-dot light-emitting diodes for display applications

Wangxiao Jin[1], Yunzhou Deng [2 ✉], Bingbing Guo[2], Yaxiao Lian[2], Baodan Zhao[2], Dawei Di [2], Xiaowei Sun[3], Kai Wang [3], Shuming Chen [3], Yixing Yang[4], Weiran Cao[5], Song Chen[6], Wenyu Ji [7], Xuyong Yang[8], Yuan Gao[9], Shuangpeng Wang[10], Huaibin Shen [11], Jialong Zhao[12], Lei Qian [13], Fushan Li[14] and Yizheng Jin [1 ✉]

Quantum dot light-emitting diodes (QLEDs) are a class of high-performance solution-processed electroluminescent (EL) devices highly attractive for next-generation display applications. Despite the encouraging advances in the mechanism investigation, material chemistry, and device engineering of QLEDs, the lack of standard protocols for the characterization of QLEDs may cause inaccurate measurements of device parameters and invalid comparison of different devices. Here, we report a comprehensive study on the characterizations of QLEDs using various methods. We show that the emission non-uniformity across the active area, non-Lambertian angular distributions of EL intensity, and discrepancies in the adopted spectral luminous efficiency functions could introduce significant errors in the device efficiency. Larger errors in the operational-lifetime measurements may arise from the inaccurate determination of the initial luminance and inconsistent methods for analyzing the luminance-decay curves. Finally, we suggest a set of recommended practices and a checklist for device characterizations, aiming to help the researchers in the QLED field to achieve accurate and reliable measurements.

INTRODUCTION

The ever-growing demands for bright, efficient, and low-cost light sources in modern society have evoked extensive interest in the research of solution-processed light-emitting diodes (LEDs). Quantum-dot LEDs (QLEDs)[1–7] are an emerging class of solution-processed electroluminescent (EL) devices using colloidal quantum dots (QDs)[8–11] as emissive materials. QLEDs feature high efficiency, tunable wavelength, narrow-band emission and compatibility with large-area or flexible substrates, representing a competitive candidate for next-generation display techonology[12–14]. In recent years, encouraging advances in operational mechanisms, material chemistry and device engineering have resulted in state-of-the-art QLEDs with external quantum efficiencies (EQE) of >25% and operation half-life of >125,000,000 h at an initial luminance of 100 cd m^{-2} (T_{95} lifetime: >300,000 h)[15–26], foreshadowing their practical implementations.

Despite the rapid developments of QLEDs, there is a lack of international standards or certificated authorities for the characterizations of emerging LED technologies. Currently, research groups employ different methods based on various optoelectronics, such as integrating-sphere photometer, goniometric photometer, or luminance meter, to characterize QLEDs. The fundamental principles and critical considerations of these

characterization methods have been discussed in several insightful articles[27–29]. Ideally, these well-established methods should be equivalent for determining the metrics of a LED. However, it is widely observed that QLEDs may show abnormal features, such as non-uniform luminance and varied angular dependency of intensity. Dependent on the choices of testing methods, these non-ideal features might induce different degrees of measurement errors in device parameters, which were less discussed in the literature.

Herein, we provide an experimental study regarding the accurate measurements of efficiency and operational lifetime of QLEDs, in which the typical characterization methods are assessed and compared. We first discuss the basic methodologies for QLED characterizations. Next, we investigate how the efficiency measurement is affected by the luminance uniformity of QLEDs, angular distribution of EL intensity of QLEDs, and the choice of spectral luminous efficiency functions. Furthermore, we address the critical considerations for the operational-lifetime measurements, including an accurate determination of the initial luminance and the extraction of lifetimes from the luminance-decay curves. Finally, we suggest a set of measurement protocols for accurate characterization of QLEDs and propose a checklist for reporting device metrics.

[1]Key Laboratory of Excited-State Materials of Zhejiang Province, State Key Laboratory of Silicon Materials, Department of Chemistry, Zhejiang University, 310027 Hangzhou, China. [2]State Key Laboratory of Modern Optical Instrumentation, College of Optical Science and Engineering; International Research Center for Advanced Photonics, Zhejiang University, 310027 Hangzhou, China. [3]Department of Electronic and Electrical Engineering, Southern University of Science and Technology, 518055 Shenzhen, China. [4]TCL Research, Shenzhen, Guangdong, China. [5]Shenzhen China Star Optoelectronics Semiconductor Display Technology Co., Ltd, Shenzhen, Guangdong, China. [6]College of Chemistry, Chemical Engineering and Materials Science, Soochow University, 199 Ren'ai Rd, 215123 Suzhou, Jiangsu, China. [7]Key Lab of Physics and Technology for Advanced Batteries (Ministry of Education), College of Physics, Jilin University, 130023 Changchun, China. [8]Key Laboratory of Advanced Display and System Applications of Ministry of Education, Shanghai University, 149 Yanchang Road, Shanghai 200072, China. [9]Najing Technology Corporation Ltd, Hangzhou 310052, China. [10]Institute of Applied Physics and Materials Engineering, University of Macau, Taipa, Macao, SAR 999078, China. [11]Key Laboratory for Special Functional Materials of Ministry of Education, National & Local Joint Engineering Research Center for High-Efficiency Display and Lighting Technology, and Collaborative Innovation Center of Nano Functional Materials and Applications, Henan University, Kaifeng 475004, China. [12]School of Physical Science and Technology, MOE Key Laboratory of New Processing Technology for Non-ferrous Metals and Materials, Guangxi Key Laboratory of Processing for Non-ferrous Metals and Featured Materials, Guangxi University, Nanning 530004, China. [13]Division of Functional Materials and Nanodevices, Ningbo Institute of Materials Technology and Engineering, Chinese Academy of Sciences, Ningbo 315201, China. [14]College of Physics and Information Engineering, Fuzhou University, Fuzhou 350108, China. ✉email: yz_deng@hotmail.com; yizhengjin@zju.edu.cn

npj

RESULTS AND DISCUSSION

Basic methodologies for the characterization of QLEDs

EQE is one of the most important parameters for fundamental research of QLEDs. For planar QLEDs with reflective electrodes designed for display applications, EQE is generally defined as the number of photons emitted into the forward-hemisphere in the viewing direction per unit time (total photon flux, Φ_p) divided by the number of electrons injected from the electrodes per unit time[30]:

$$\text{EQE }(\%) = \frac{\Phi_p}{I/e} \tag{1}$$

where I and e represent the current and elementary charge, respectively. EQE provides a measure of the quantum yield of EL processes of a QLED and enables a direct comparison between devices with different emission wavelengths.

In addition to EQE, current efficiency (CE) is another important parameter widely used in the display industry. CE is defined as the luminous intensity in the normal direction ($I_v(0°)$, luminous flux per solid angle) divided by the input current, or equivalently, the luminance in the normal direction (L_v, luminous intensity per area) divided by the current density:

$$\text{CE}\left(cdA^{-1}\right) = \frac{I_v(0°)}{I} = \frac{L_v}{I/A} \tag{2}$$

where A is the active area of the QLED. Besides, luminous efficiency (output luminous flux per electrical input power, lm/W) and power-conversion efficiency (optical output power per electrical input power, %) are also key parameters for the performance evaluation of EL devices[31].

According to Eqs. (1) and (2), the efficiency characterization of a QLED requires simultaneous measurements on both the electrical parameters and the optical parameters. For the voltage-sweep measurements, the control program should enable synchronized reading of optical signals with electrical signals during each voltage step. Given that the electrical parameters (current and voltage) can be readily measured by using a high-precision source meter, the major challenges for efficiency characterizations of QLEDs lie in the accurate measurements of the optical parameters including the total photon flux and the luminous intensity (or the luminance).

The total photon flux of a QLED (Φ_p) is derived either from the spectral radiant flux ($\Phi_e(\lambda)$, unit: W) or from the spectral luminous flux ($\Phi_v(\lambda)$, unit: lm) with the knowledge of the emission spectrum, according to the equation of:

$$\Phi_p = \int \frac{\Phi_e(\lambda)}{hc/\lambda} d\lambda \tag{3}$$

$$\Phi_e(\lambda) = \frac{\Phi_v(\lambda)}{K_m \cdot V(\lambda)} \tag{4}$$

where h, c and λ represent the Plank constant, the speed of light in vacuum, and the wavelength of emitted photons, respectively. $V(\lambda)$ is the standard spectral luminous efficiency function (Supplementary Table 1) that describes the relative spectral sensitivity of human eyes to light at different wavelengths. K_m is the maximum luminous efficacy corresponding to the wavelength of 555 nm (683 lm/W). According to Eq. (4), radiometric measurements (signals response to Φ_e) or photometric measurements (signals response to Φ_v) are in principle equivalent.

The luminous intensity and the luminance of a QLED can be directly measured by photometric methods. Considering that QLEDs generally exhibit axial-symmetric-intensity characteristics, the luminous intensity is connected with the total luminous flux through the equation of:

$$\Phi_v = \int I_v \cdot d\Omega = \int_0^{\pi/2} 2\pi \cdot I_v(\theta) \sin\theta \, d\theta \tag{5}$$

where θ is the viewing angle with respect to the direction perpendicular to the device surface. For QLEDs with

bottom-emitting architectures (with no strong microcavity structure), it is often observed that the devices exhibit Lambertian-type angular distribution of EL intensities, i.e., the luminous intensity varies as the cosine function of the viewing angle:

$$I_v(\theta) = I_v(0°) \cdot \cos\theta \tag{6}$$

under the Lambertian approximation, the luminous intensity in the normal direction and the luminance can be derived from the total luminous flux according to a reduced form of integration:

$$\Phi_v = \int_0^{\pi/2} 2\pi \cdot I_v(0°) \cdot \cos\theta \cdot \sin\theta d\theta = \pi \cdot I_v(0°) = \pi \cdot L_v \cdot A \tag{7}$$

according to the LED-characterization standards issued by the International Commission on Illumination (CIE)[32] and the Illuminating Engineering Society of North America (IESNA)[33], there are three basic methodologies for measuring the total luminous flux (or radiant flux) and the luminous intensity of LEDs (Fig. 1):

1. Integrating-sphere photometer: directly measures the total luminous flux.
2. Goniometric photometer: measures the distribution of luminous intensity as a function of viewing directions, from which the total luminous flux is calculated.
3. Luminance meter: measures the luminance of a small region of the device in the normal direction, from which the luminous intensity in the normal direction, as well as the total luminous flux, is calculated.

Below we briefly discuss the principles and instruments of the three methodologies. A comparison of the three basic methods is summarized in Table 1.

Integrating-sphere photometer

Integrating-sphere photometer is a common instrument for measuring the total luminous flux (or radiant flux) of luminaires. An integrating-sphere photometer composes of a light-collection unit of an integrating sphere coupled to a photodetector. The integrating sphere is an optical component consisting of a hollow cavity with diffuse reflectance coatings on the inner surface, enabling uniform scattering of the photons emitted from a light source. For QLEDs with typical planar configurations, a "2π geometry" of the experimental set-up is used to collect all the photons emitting to the forward hemisphere[34], in which the plane of device substrate is above the entrance port of the integrating sphere. To strictly prevent the collection of the light emitted from the substrate edges, we suggest that the diameter of the entrance port should be considerably smaller than the diameter of the device substrate (Supplementary Fig. 1). Besides, the accessories of the integrating-sphere photometer (e.g., the device holder and the electrical probe) must be appropriately designed to ensure that edge emission is not back-scattered into the sphere. Owing to the multiple diffuse reflections inside the sphere, the indirect illuminance (or irradiance) on the inner wall is proportional to the total collected luminous flux (or radiant flux). Thus, the total luminous flux of a QLED can be obtained by using a cosine-corrected collection port (i.e., the sensitivity independent of the angle of incidence) coupled to a photodetector. A built-in baffle is often used to block the direct incident light from the QLED at the collection port (Supplementary Fig. 1 for the design of integrating-sphere).

We note that a '4π geometry' set-up, in which the LED is placed at the center of the integrating sphere, can also be employed to characterize QLEDs[34]. In addition to the photons emitted into the forward-hemisphere of the QLED, a large fraction of photons collected by the '4π geometry' set-up is contributed by the waveguided light emitted from the edges of the substrates. Thus, the results measured by the '4π geometry' set-up are considerably higher than those measured by using the '2π geometry'. To avoid ambiguities in the comparisons of efficiencies, we suggest the
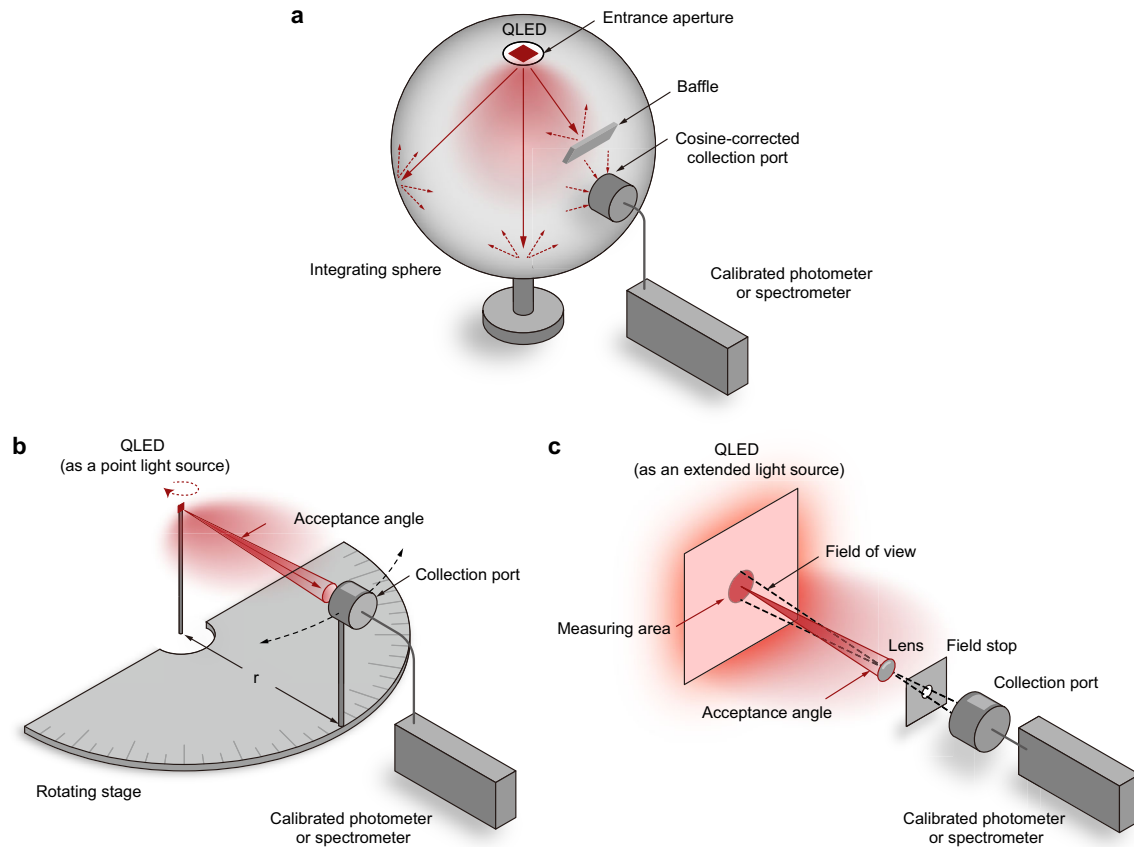
Fig. 1 Experimental set-ups of three basic methods for efficiency characterizations of QLEDs. a Integrating-sphere photometer measures all lights emitted into the forward hemisphere of the device. The '2π geometry' as shown by the schematic is recommended for measuring the display-relevant efficiencies of planar QLEDs. **b** Goniometric photometer measures light intensity in a small solid angle (denoted as the acceptance angle) as a function of viewing angle. The angular-dependent measurement is realized by revolving the detector around the fixed QLED (black dashed arrows) or by rotating the QLED (red dashed arrows). **c** Luminance meter measures the luminance in a small region of the device in the normal direction.

researchers state the specific experimental set-up used for the integrating-sphere photometer. Moreover, for the measurements of display-relevant EQEs (forward-viewing directions), we recommend using the '2π geometry' to characterize the planar QLEDs[29].

In EQE measurements, either a CCD spectrometer or a $V(\lambda)$-calibrated photodiode (i.e., relative spectral responsivity identical to $V(\lambda)$) can be employed as the photodetector. The CCD spectrometer enables a direct and fast measurement of the spectral radiant flux (or spectral luminous flux) of the device. By comparison, the Si-photodiodes generally offer a wider dynamic range ($>10^6$) and better linearity in response, which is advantageous for characterizing QLEDs operated at different luminance levels.

For the integrating-sphere photometer using a spectrometer as the detector, the total spectral luminous flux is determined directly from the spectrometer signals ($S(\lambda)$, unit: counts nm^{-1}) according to the equation of:

$$\Phi_v(\lambda) = S(\lambda)/R_v(\lambda) \tag{8}$$

where $R_v(\lambda)$ is the absolute spectral responsivity of the spectrometer (unit: counts lm^{-1} nm^{-1}) calibrated with a luminous-flux standard lamp. Analogously, the total spectral radiant flux of the testing device ($\Phi_e(\lambda)$) can be directly measured if a radiant-flux standard lamp is used for calibration of the absolute spectral responsivity of the spectrometer ($R_e(\lambda)$, unit: counts W^{-1} nm^{-1}). Based on the Lambertian assumption, the luminous intensity and

the luminance in the normal direction of the QLED can be further derived from the measured total luminous flux by using Eq. (7).

A major advantage of using the integrating-sphere photometer is the capability of direct determination of total luminous flux (or radiant flux) in the forward hemisphere for EQE measurements. The measurements of the luminance and the CE by using an integrating-sphere photometer are indirect and require the knowledge of angular dependency of EL intensity (see the section of Angular distribution of emission on efficiency characterizations) or the use of Lambertian approximation to derive the photometric quantities in the normal direction. We recommend that the integrating-sphere photometer should be calibrated regularly because several factors, such as accidental contamination of the integrating sphere, minor changes in the optical adapters, or mechanical drifts of the spectrometer, may cause errors. We note that the calibration of the absolute responsivity of an integrating-sphere photometer using Si-photodiodes as the detector is not trivial, and great care must be taken to calibrate the spectral mismatch factor of the system. The practices for rigorous calibration of an integrating-sphere photometer are provided in Supplementary Notes 1, 2 and Supplementary Fig. 1.

Goniometric photometer

A goniometric photometer is a device to measure the luminous intensity and the luminance of a light source at different viewing

Table 1. Comparison of three methodologies for the efficiency measurement of QLEDs.

Method	Integrating-sphere photometer (2π geometry)	Goniometric photometer	Luminance meter
Measured quantity	Total luminous (or radiant) flux	Luminous (or radiant) intensity in the different viewing directions	Luminance (or radiance) in a specified area in the forward direction
Key components	Integrating sphere with a built-in baffle and a cosine-corrected collection port	A stable and precisely positioned rotating stage	Imaging optics with a field stop
Requirements on the sample size	Less than 1/3 of the inner diameter of the integrating sphere	<1/5 of the measuring distance	Larger than the measurement field
Basic Assumptions	Uniform distribution of illuminance inside the sphere	Point light source; Lambertian emission pattern (for the simplified method)	Extended light source; Uniform luminance; Lambertian emission pattern
Advantages	Fast and direct measurement of the total luminous flux.	A complete profile of angular-dependent luminescent properties; Fast and direct measurement of the luminance; High light-detection efficiency for low-luminance measurements.	Fast and direct measurement of the luminance.
Disadvantages	Lack of angular information; Relatively lower detection efficiency.	Angular-dependent measurement is time-consuming; High requirements on the optical and mechanical components.	Requires multiple measurements to cover the entire device area; Lack of angular information.

directions (Fig. 1b). Either a spectrometer or a $V(\lambda)$-calibrated photodiode can be employed as the detector in a goniometric photometer. The measurement of the luminous intensity by using a goniometric photometer requires the EL device to be treated as a point light source. To fulfill this assumption, the dimension of the luminous surface should be negligible compared with the measuring distance from the device to the detector. It is recommended by the CIE standard that the measuring distance should be at least 5 times greater than the largest dimension of the LED[32]. The angular-dependent measurements can be conducted by revolving the detector around the fixed QLED (black dashed arrow), or by rotating the QLED with the detector fixed (red dashed arrow). The total spectral luminous flux (or total spectral radiant flux) of QLEDs can be measured by integrating the luminous-intensity distributions as a function of viewing directions (I_v) according to the equation of:

$$\Phi_v(\lambda) = \int_0^{\pi/2} 2\pi \cdot I_v(\theta, \lambda) \sin\theta \, d\theta = \int_0^{\pi/2} 2\pi \cdot S(\theta, \lambda) \sin\theta / R_v(\lambda) \, d\theta \tag{9}$$

where θ is the viewing angle with respect to the direction perpendicular to the device surface, $R_v(\lambda)$ is the absolute spectral responsivity of the spectrometer (unit: counts cd^{-1} nm^{-1}), and $S(\theta, \lambda)$ is the spectrometer signals (unit: counts nm^{-1}).

Characterizing the complete luminous intensity distributions over 90° of viewing directions is time-consuming and demands precise rotary motions of the detector or the device. In practice, these procedures are often simplified by assuming the QLED to be a Lambertian emitter (Eq. (6)), and the determination of the total spectral luminous flux only requires the measurement in the normal direction (spectrometer signal: $S(0°, \lambda)$) according to Eq. (7):

$$\Phi_v(\lambda) = \pi \cdot S(0°, \lambda) / R_v(\lambda) \tag{10}$$

for the absolute measurement of luminous intensities, the $R_v(\lambda)$ of the goniometric photometer should be calibrated by using a luminous-intensity standard lamp. In the simplified measurements of total luminous flux (or total radiant flux) based on the Lambertian assumption, the system can be calibrated by using a total-luminous-flux standard lamp (or total-radiant-flux standard lamp) with a Lambertian emission pattern. Similar to the case with an integrating-sphere photometer, care shall be taken when dealing with the complex calibration of the spectral

mismatch factor when a photodiode is used as the detector in the goniometric-photometer setup.

One of the goniometric photometer's advantages is the capability of acquiring a complete profile of luminescent properties in various viewing directions, also enabling direct measurements of the luminance as well as the CE of a QLED. Moreover, the goniometric photometer generally possesses higher light-detection efficiency than that of the integrating-sphere photometer, owing to the direct detection of light emitted from the device with no additional diffuser (e.g., low-transmittance cosine corrector) equipped on the detection head. The high sensitivity makes goniometric photometers suitable for characterizing QLEDs operating at low-injection conditions. The measurement of EQE by using the goniometric photometer demands the integration of angular-dependent signals or the use of a Lambertian assumption. This method has high requirements on the instruments with regard to the positioning accuracy, motion reliability, and suppression of stray lights. Besides, accurate measurements of light intensities at large viewing angles are challenging owing to the decreased signal-to-noise ratio and the spatial blocking by mechanical components. Also, it should be ensured that the waveguided lights emitted from the substrate of the QLED are blocked and should not enter the detector. These critical considerations have been discussed in detail in a previous report[27].

Luminance meter

A luminance meter is widely-used photometric apparatus for directly characterizing the extended light source by the luminance. The luminance meter also provides a solution to determine the total luminous flux (or total radiant flux) of LEDs. Distinctive from the integrating-sphere photometer and the goniometric photometer, the luminance meter collects light from a small area of the emitting device and measures the luminance in this small field of view (Fig. 1c). The absolute luminance is calibrated by using a luminance-standard source with a uniform luminous. The area of the light source should be considerably larger than the measurement field.

In principle, two critical requirements of the QLED, i.e., a spatially uniform distribution of luminance and a known angular-dependence of luminous intensities (e.g., a Lambertian emission pattern), should be met to enable the measurement of total

luminous flux with a luminance meter. For the QLED with a uniform distribution of luminance in the device area, the average luminance of the device is equal to the local luminance measured from a specified small region ($L_v(x, y)$). Thus, the overall luminous intensity in the normal direction is obtained by multiplying the device area:

$$I_v(0°) = L_v(x, y) \cdot A \tag{11}$$

by further assuming that the testing QLED possesses a Lambertian emission pattern, as described in Eq. (7), the total luminous flux can be derived from the measured luminance by a reduced form of

$$\Phi_v = \pi \cdot L_v(x, y) \cdot A \tag{12}$$

Operation-lifetime measurement

The operation stability of QLEDs is generally evaluated by measuring the evolution of the luminance of a device driven at a constant current density. The operation lifetime (e.g., T_{95} or T_{50}) is defined by the time when the relative luminance decays to a defined threshold (e.g., 95% or 50%) of the initial luminance. Since the initial luminance is often pre-determined from the efficiency measurements by using the methods discussed above, simple optics are used to track the relative luminance of a QLED.

The luminance-decay characteristics of a LED are strongly dependent on the electrical-excitation level, i.e., the higher the current density (or the initial luminance), the shorter the operation lifetime[35]. The operation lifetimes at an initial luminance of 100 or 1000 cd m^{-2} (calibrated by efficiency measurement) are often used for the evaluation and comparison of device stabilities for display applications. For state-of-the-art QLEDs with high operational stabilities, a complete operational-lifetime measurement at a low initial luminance can be time-consuming for fundamental research (e.g., T_{50}@100 cd m^{-2} > 100,000 h). Practically, the operational lifetime corresponding to a lower initial luminance ($T(L_0)$) can be extrapolated from acceleration tests at higher initial luminance according to an empirical scaling law of ref. [35,36]:

$$L_0^n \cdot T(L_0) = \text{constant} \tag{13}$$

where n is the empirical acceleration factor. The acceleration factor of the QLED can be obtained from a power-law fitting of the relation between the measured lifetimes and the corresponding initial luminance. Literature results show that the typical values of acceleration factors for QLEDs are in the range of 1.5–2[13]. The variations of the acceleration factors of QLEDs might be due to the different material properties and degradation mechanisms.

Besides, experience from inorganic LEDs and organic LEDs shows that the operational lifetimes can be projected by fitting the luminance-decay curves of relatively short durations. A widely accepted empirical law that describes the effects of intrinsic degradation of LEDs on the luminance decay (L_t) is the stretched-exponential decay model[35–37]:

$$\frac{L_t}{L_0} = \exp\left[-\left(\frac{t}{\tau}\right)^\beta\right] \tag{14}$$

where L_0 is the initial luminance, τ is the decay constant that depends on the current density, and β is the stretching factor correlated to the materials but independent of the current density. Accordingly, the projected by using the linear relation between $\log[\ln(L_0/L_t)]$ and $\log(t)$:

$$\log[\ln(L_0/L_t)] = \beta\log(t) - \beta\log(\tau) \tag{15}$$

Luminance uniformity on efficiency characterizations

The above discussions on the measurements of QLED efficiencies suggest that special attention should be paid to the assumptions made for the respective methods (Table 1). While the integrating-sphere photometer is the most direct and universal method to measure the total luminous flux as well as the EQE, other characterization methods are generally based on the assumptions of uniform luminance in the device area or known emission patterns. Accordingly, we investigate the impacts of spatial distributions of luminance and angular distributions of intensity on the characterization of QLEDs.

QLEDs could exhibit non-uniform distributions of luminance across the device area owing to the material impurities, defects induced in device preparation, or uneven film morphology at the edges of the electrodes. Furthermore, we emphasize that many high-efficiency QLEDs relied on a 'positive-ageing' process to improve the device performance during the initial storage, which is resulted from the in-situ reactions induced by the acidic resins used for encapsulation[38,39]. The use of acidic resins can further increase the non-uniformity of the luminance of a QLED owing to the etching of the cathodes by the residue acids in the resin or the by-products of the in-situ reactions (e.g., water) accumulated in the devices[25].

We prepared three red QLEDs with different degrees of luminance non-uniformity to investigate the impacts of the luminance uniformity of a QLED on the accuracy of EQE characterizations. Figure 2a–c shows the corresponding microscopic images of the three working QLEDs (denoted as Device A, Device B, and Device C). Overexposure in the acquirement of microscopic images was avoided to prevent possible underestimation of the luminance uniformity (Supplementary Fig. 2). Device A possesses a uniform distribution of luminance in the device area and Device B and Device C show pronounced dark regions. We use the relative standard deviations of the brightness in the device area (RSD_L), i.e., normalized indicators describing the widths of the histograms of brightness (Fig. 2a–c, right), to quantify the luminance non-uniformities of these QLEDs. Device A, Device B, and Device C show RSD_L of 0.10, 0.39, and 0.59, respectively.

An integrating-sphere photometer and a luminance meter (measurement field area: ~0.3 mm^2) were employed to measure the EQE of three devices (driven at current densities of 10 mA cm^{-2}), respectively. The results of the integrating-sphere photometer (EQE_{IS}) are 19.1%, 20.0%, and 20.2% for Device A, Device B and Device C, respectively. Regarding the measurements with the luminance meter, we conducted parallel tests at 16 different positions (driven at current densities of 10 mA cm^{-2}) on each device. During the 16 tests on each device (within 10 min), no noticeable degradation in QLEDs was observed. The resulting EQE values (EQE_{LM}) are shown in Fig. 2d–f.

We compare the EQE_{LM} values with the EQE_{IS} for each device (Fig. 2g–i). While the average EQE_{LM} values from 16 positions of each device roughly agree with the corresponding EQE_{IS} values (averaged EQE_{LM}: 19.1%, 21.0%, and 21.4% for the three devices, respectively), the spatial deviations of the EQE_{LM} values increase as the luminance non-uniformity of the QLED increases (shaded regions in Fig. 2g–i). We note that EQE_{LM} values exceeding the limit of out-coupling efficiencies of our devices (e.g., EQE_{LM} > 40%) are obtained at a few positions.

Further measurements on 27 QLEDs verify the positive correlation between the luminance non-uniformity and the spatial deviations of EQE_{LM}. In Fig. 3, the variations of the EQE_{LM} values obtained at 16 different positions for each QLED is plotted against the RSD_L of the respective device. An increase in the non-uniformities of QLEDs leads to larger RSD of the EQE_{LM} values, indicating an increased uncertainty for the EQE characterizations based on the luminance meter.

The above results highlight the differences between integrating-sphere photometer and luminance meter in the EQE measurements. The accuracy of the integrating-sphere based measurement is not affected by the luminance non-uniformity of
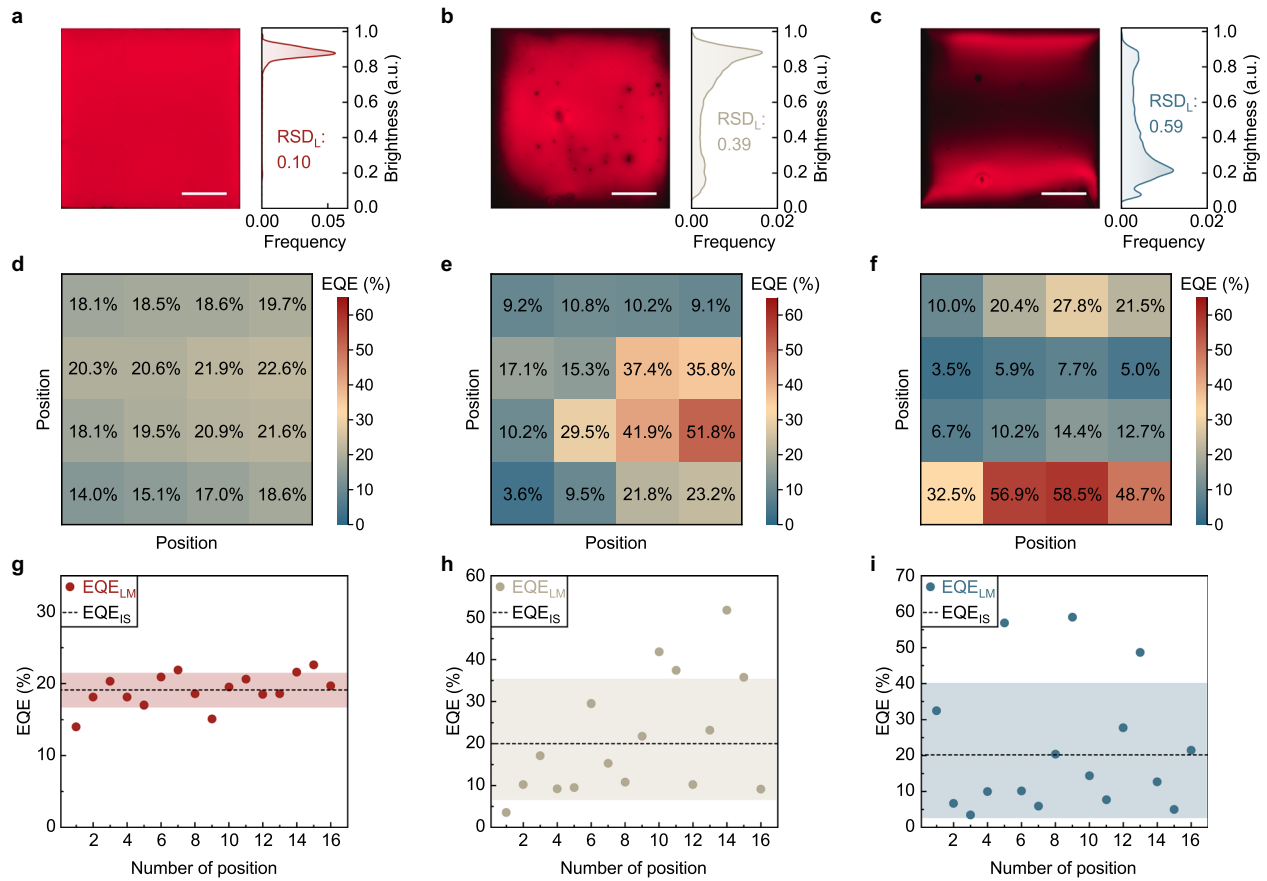
Fig. 2 Impacts of luminance non-uniformity of QLEDs on the efficiency measurements. a–c Microscopic images (left, scale bar: 0.5 mm) and the corresponding histograms of brightness distributions (right) of the three operating QLEDs with different luminance uniformities. **d–f** EQE values measured at different detecting positions of the three QLEDs (shown in **a–c**, respectively) by using a luminance meter with a field area of ~0.3 mm². **g–i** Comparisons of the EQE values measured with the luminance meter (EQE_LM, circles) and the EQE measured with the integrating-sphere photometer (EQE_IS dashed lines) for the three QLEDs. The shaded region is defined by the average value and the standard deviations of EQE_LM for each device.
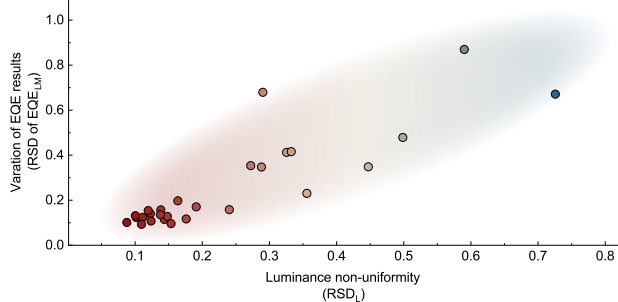

Fig. 3 Correlation between the uncertainty of efficiency measurements using a luminance meter and luminance non-uniformity of the QLEDs. Efficiency measurements were performed on 27 QLEDs with different degrees of luminance uniformity by using a luminance meter. The uncertainty of efficiency measurements for each device is determined from the relative standard deviations of 16 EQE_LM values obtained at different positions, as shown in Fig. 2d–f.

the QLED because all the photons emitted from the entire device area are detected. This also holds for goniometric-photometer-based measurement, in which the QLED is treated as a point light source. In contrast, for the luminance-meter based measurement, results are largely affected by the luminance non-uniformity

because the detecting field for the emitting photons is smaller than the device area while the total current flowing through the whole device area is measured. Thus, the spatial distribution of EQE_LM values has a strong correlation with the distribution of luminance uniformity. Moreover, control experiments show that the variations of EQE_LM values for Device B and Device C are still pronounced even when a wider measurement field area (~1.2 mm², more than a quarter of the device area) is applied for the measurements (Supplementary Fig. 3). Moreover, the non-uniform luminance in the QLED might be resulted from spatial variations of the current densities in the device area. Consequently, additional errors might be introduced into the EQE_LM values for the regions where the local current densities deviate from the average current density.

Given the critical impacts of luminance uniformity on the EQE measurements using luminance meter, accurate determination of the device EQE by a luminance meter would require multiple measurements to cover the entire device area. Thus, we recommend that for EQE measurements by a luminance meter, both the luminance distributions and the spatial variations of EQEs shall be reported. Overall, for QLEDs with non-uniform luminance, the integrating-sphere photometer or goniometric photometer may be more reliable approaches for the EQE characterizations. We also note that for these QLEDs, the luminance measured with the integrating-sphere photometer or goniometric photometer represents the averaged luminance across the device area.
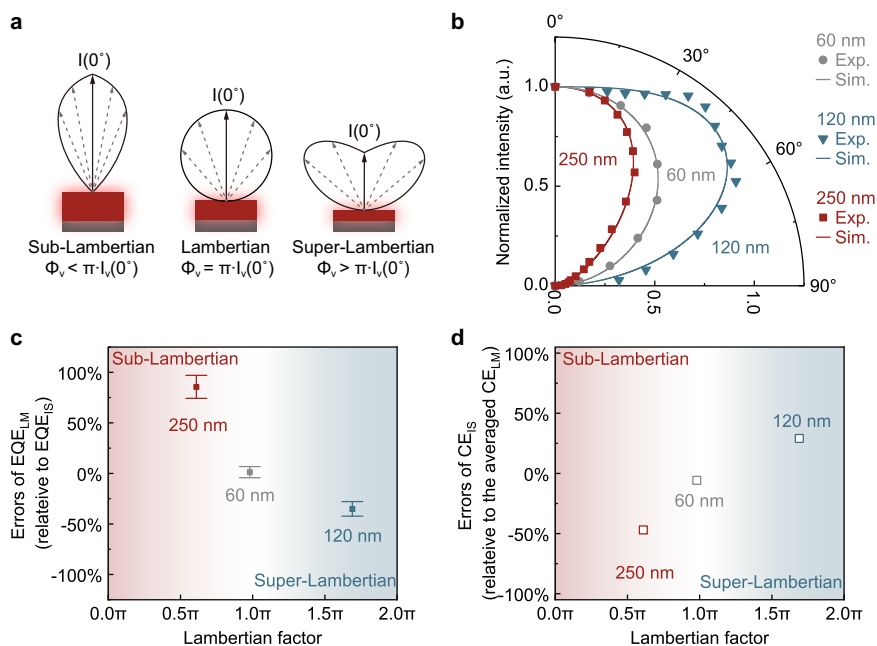
Fig. 4 Impacts of the angular distribution of EL intensity of QLEDs on the efficiency characterizations. a Schematic diagrams showing that varying the microcavity lengths of the QLEDs could result in different types of emission patterns. The light intensities are illustrated by the lengths of the arrows. **b** Light intensity as a function of viewing angle for QLEDs with the thickness of ZnMgO electron-transporting layers being 60 nm (gray), 120 nm (blue) and 250 nm (red), respectively. The optical simulation results for the emission patterns of the three devices are displayed by the solid lines. The 0° direction corresponds to the normal direction of the device plane. **c** Relative errors of the EQEs measured with a luminance meter (EQE_{LM}) compared with those measured with an integrating-sphere photometer (EQE_{IS}) for the three QLEDs with different emission patterns. The squares and bars represent the average values and relative standard deviations of 16 EQE_{LM} values at different positions of each device, respectively. **d** Relative errors of the CEs measured with an integrating-sphere photometer (CE_{IS}) comparing with the averaged CEs measured with a luminance meter (CE_{LM}) for the three QLEDs. The squares and bars represent the average values and relative standard deviations of 16 CE_{LM} values at different positions of each device, respectively.

Angular distribution of emission on efficiency characterizations

Angular distributions of the intensity of state-of-the-art QLEDs are often assumed to be Lambertian patterns in EQE characterizations. However, the actual emission pattern of a LED is determined by multiple optical effects and can exhibit non-Lambertian characteristics[27,40] (Fig. 4a). Specifically, our optical simulations demonstrate that the emission pattern of QLEDs is mainly governed by the microcavity length of the device and thus, variations of the thickness of $Zn_{0.9}Mg_{0.1}O$ electron-transport layers functional layers can lead to deviations from the Lambertian characteristics (Fig. 4b).

To evaluate the deviation of angular distribution from the Lambertian pattern, we define the Lambertian factor of a QLED as:

$$\text{Lambertian factor} = \frac{\Phi_v}{I(0)} = \frac{\int_0^{\pi/2} 2\pi \cdot \sin(\theta) I_v(\theta) d\theta}{I_v(0^\circ)} \quad (16)$$

an ideal Lambertian emitter is characterized by a Lambertian factor of π, which is used to calculate the efficiency in luminance-meter based measurements (Eq. (12)). Simulation results show that as the thickness of $Zn_{0.9}Mg_{0.1}O$ increases from 70 to 250 nm (or decreased from 60 to 25 nm), the intensity distribution changes from the 'super-Lambertian' characteristics, i.e., side-direction dominated (Lambertian factor $> \pi$), to the 'sub-Lambertian' characteristics, i.e., forward-direction dominated emission (Lambertian factor $< \pi$). Notably, an ideal Lambertian emission pattern can only be achieved in a small window of $Zn_{0.9}Mg_{0.1}O$ thickness (Supplementary Fig. 4).

Invalid Lambertian approximation for the QLEDs with non-Lambertian characteristics leads to errors in the conversion between the total luminous flux and the luminous intensity in the normal direction. This is verified by our comparison of characterization results by using a luminance meter or using an integrating sphere. Three QLEDs with $Zn_{0.9}Mg_{0.1}O$ thicknesses of 60, 120, and 250 nm, respectively, were fabricated, which exhibit uniform luminance in the active regions ($RSD_L < 0.10$). Angular-dependent EL-intensity measurements demonstrate the distinctive emission patterns of these QLEDs (scatters, Fig. 4b) with the Lambertian factors being 1.0π (60 nm), 1.7π (120 nm), and 0.6π (250 nm), respectively, which agrees well with the simulation results (lines, Fig. 4b). The EQEs of the devices measured with the integrating-sphere photometer, EQE_{IS}, which collects all the emitting photons in the forward hemisphere regardless of the angular distributions, are determined to be 16.3%, 15.1%, and 11.8%, respectively. For the device with Lambertian characteristics, the average EQE_{LM} is close to EQE_{IS} (Fig. 4c, middle). In contrast, for the devices with non-Lambertian characteristics, there are considerable discrepancies between the average EQE_{LM} and EQE_{IS}. Specifically, a sub-Lambertian emission pattern causes an overestimation of both the total luminous flux and the EQE (Fig. 4c, left) in the luminance-meter-based measurement, while a super-Lambertian emission pattern causes an underestimation of both the total luminous flux and the EQE (Fig. 4c, right). The extent of the measurement error correlated well with the deviations of the Lambertian factors from π. Analogous to the errors in EQEs, invalid Lambertian approximation might induce errors in the CE values measured with the integrating-sphere photometer (CE_{IS}), which are derived from the total photon flux by using the Lambertian approximation (Eq. (7)). Figure 4d shows a comparison of the CE_{IS} and the accurate CEs measured with the luminance meter (CE_{LM}). While the CE_{LM} agrees with the CE_{IS} for the QLED with Lambertian emission pattern, there is an overestimation in the CE_{IS} for the QLED with a super-Lambertian emission pattern and an underestimation in the CE_{IS} for that with a sub-Lambertian emission pattern.
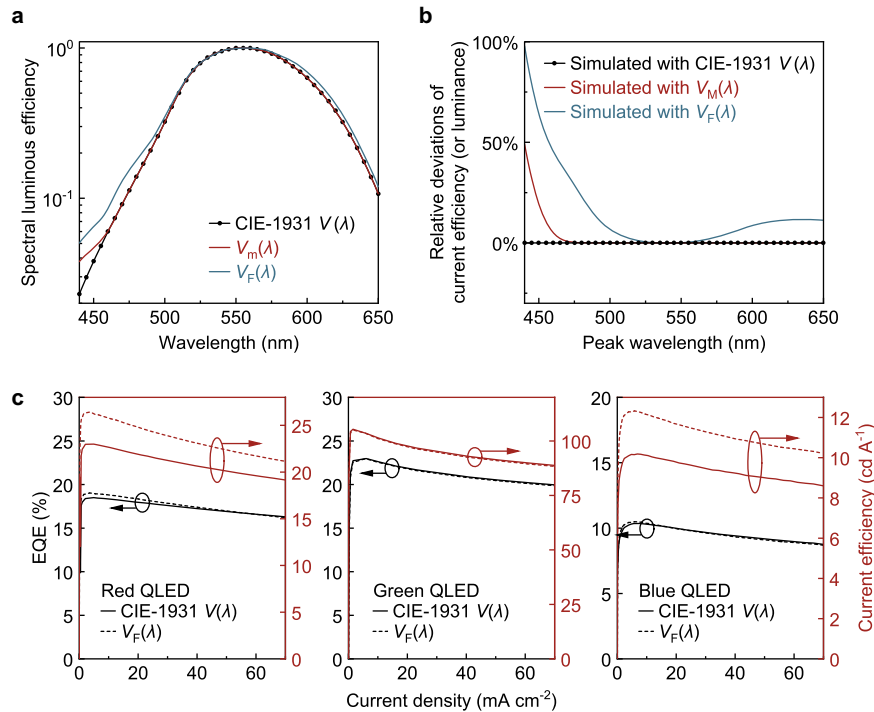
Fig. 5 Measurement deviations caused by adopting different versions of spectral luminous functions. a Comparison of three spectral luminous efficiency functions. $V(\lambda)$ is the current international standard (CIE-1931). $V_M(\lambda)$ and $V_F(\lambda)$ are the Judd–Vos modified spectral luminous efficiency function and the 'physiologically relevant' spectral luminous efficiency function, respectively, which show higher values in the red and blue spectral region comparing with $V(\lambda)$. **b** Simulation on the relative deviations of the measured luminance of QLEDs caused by using different spectral luminous functions of $V_M(\lambda)$ (red curve) or $V_F(\lambda)$ (blue curve). The simulated luminance values by using CIE-1931 $V(\lambda)$ are shown for comparison (black line). **c** EQE and current efficiency results of the red (left), green (middle) and blue QLEDs (right) QLEDs. Two sequential measurements were conducted on each device, in which $V(\lambda)$ (solid curves) or $V_F(\lambda)$ (dashed curves) were used to calculate the luminance from the radiant flux, respectively.

The above results suggest that it is necessary to characterize the angular distributions of the EL intensity before the efficiency measurement. In the report of device metrics, we also recommend the researchers provide an explicit statement on whether a Lambertian assumption is made in the efficiency characterization. For QLEDs with non-Lambertian emission patterns, the EQE values calculated from the luminous intensity (or luminance) measured in the normal direction (e.g., EQE_{LM}), or the CE values calculated from the total luminous flux measured in the forward-hemisphere (e.g., CE_{IS}), can be corrected by using the measured Lambertian factor:

$$EQE = EQE_{LM} \cdot \text{Lambertian factor}/\pi \qquad (17)$$

$$CE_v = \pi \cdot CE_{v,IS}/\text{Lambertian factor} \qquad (18)$$

we note that additional difficulties in the measurement could arise from the variation in the EL spectra at different viewing directions, which is commonly observed for top-emitting QLEDs with wide-band emissions (see Supplementary Fig. 5 for the example). The EL spectrum in the normal direction of these QLEDs can be significantly different from the overall EL spectrum in the forward-hemisphere. Thus, the luminance and the CEs of these QLEDs cannot be directly determined by using the integrating-sphere photometer. Regarding the EQE measurement, it is infeasible to characterize the total photon flux of these QLEDs by using a luminance meter or a photodiode-based goniometric photometer because the overall EL spectrum in the forward hemisphere cannot be obtained. Overall, for the QLEDs with angular-dependent EL spectra, we recommend the use of luminance meter or goniometric photometer to characterize the CEs, and the use of integrating-sphere photometer or spectrometer-based goniometric photometer (with angular-dependent measurement) to characterize the EQEs.

Deriving luminance from radiometric quantities

In addition to the instrumental considerations, the reliability of efficiency characterizations is also affected by data-processing procedures. A general procedure in optical measurements is the conversion between radiometric quantities (e.g., radiant flux) and photometric quantities (e.g., luminous flux). For a measurement system calibrated by using a standard lamp with known radiometric quantities, the luminance value (or luminous intensity value) of the QLED is derived from the measured radiant flux (or radiant intensity) through the spectral luminous efficiency function $V(\lambda)$ (Eq. (4)).

We highlight the existence of various versions of $V(\lambda)$ causes ambiguities for QLED characterizations. The current international standard is the CIE-1931 $V(\lambda)$ function (Supplementary Table 1), which is also endorsed by The International System of Units (SI system) that defines photometric units[41,42]. Besides this function, other modified spectral luminous efficiency functions, such as the Judd-Vos modified function $(V_M(\lambda))$[43,44] and the physiologically relevant function consistent with the cone fundamentals $(V_F(\lambda))$[45–47], have also been endorsed by CIE (Supplementary Table 2). Detailed information on the development of the $V(\lambda)$ is provided in Supplementary Note 3. We are aware that different versions of $V(\lambda)$ have been adopted in the literature on solution-processed LEDs[27,28]. Owing to the discrepancies of these $V(\lambda)$ functions (Fig. 5a), inconsistent use of $V(\lambda)$ in literature reports may induce systematic deviations in the characterization results.

We analyze the wavelength-dependent impacts of discrepancies in $V(\lambda)$ on the determination of luminance of QLEDs by simulation. In the simulation, EL spectra of QLEDs were assumed to be Gaussian peaks with a fixed full-width at half-maximum of 25 nm. The relative deviations of the luminance measured by using the modified $V(\lambda)$ (Fig. 5b) were compared with that

measured by using standard CIE-1931 $V(\lambda)$. The results suggest that the use of $V_M(\lambda)$ shall cause an overestimation of the luminance (>5%) at wavelengths shorter than 460 nm (red line, Fig. 5b). When using $V_F(\lambda)$, the overestimation of the luminance could be greater than 10% or 20% in the red spectral range (610–650 nm) or the blue spectral range (<480 nm), respectively. These results originated from the higher values of the modified $V(\lambda)$ in the blue and the red-orange spectral ranges, compared with those of CIE-1931 $V(\lambda)$ (Fig. 5a).

The above trend is experimentally verified by the characterization of red (629 nm), green (536 nm), and blue (479 nm) QLEDs with a radiant-flux-calibrated integrating-sphere photometer. Two series of measurements were conducted on each device, in which the standard CIE-1931 $V(\lambda)$ and the modified $V_F(\lambda)$ were, respectively, applied to calculate the performance metrics (Fig. 5c). The EQE results remain unchanged because the photon flux is directly derived from the measured total spectral radiant flux ($\Phi_e(\lambda)$, see Eq. (3)). Regarding the CEs that are correlated with luminance, the measurement results for the blue and red QLEDs using $V_F(\lambda)$ (peak: 12.3 and 26.4 cd A^{-1}, respectively) are considerably higher than those using standard CIE-1931 $V(\lambda)$ (peak: 10.2 and 23.0 cd A^{-1}, respectively).

Our survey on the previous reports of high-performance QLEDs at similar wavelengths suggests that there are discrepancies in the ratios of CE to EQE (CE–EQE ratios) (Supplementary Fig. 6). Some of the CE–EQE ratios deviated from the theoretical values predicted according to the EL spectra and the standard CIE-1931 $V(\lambda)$. These facts suggest the inconsistency in the choices of spectral luminance efficiency functions in the QLED community.

We recommend that the standard CIE-1931 $V(\lambda)$ shall be applied in the characterizations of QLEDs. Despite that $V_M(\lambda)$ and $V_F(\lambda)$ functions represent recent advances in vision science and physiology, they have not been recognized by International Committee for Weights and Measures (CIPM)[18]. Thus, we do not recommend the use of $V_M(\lambda)$ and $V_F(\lambda)$ functions as standards for photometric measurements. Given that the misinterpretation of the initial luminance shall cause amplified errors in the operation lifetime (see the section below), strictly applying the standard CIE-1931 $V(\lambda)$ shall further enable valid comparisons of the operation lifetime of QLEDs.

Determine initial luminance for lifetime characterizations

The accuracy of operation-lifetime measurements can be significantly affected by the error of the measurements of the initial luminance derived from the efficiency characterizations. According to the power-law relation of Eq. (13), a 10% overestimation of the initial luminance can lead to a ~20% overestimation of the operation lifetime at the corresponding nominal initial luminance (assuming an acceleration factor of 1.9). Therefore, for accurate measurements of operation lifetime, it is critical to avoid the errors and uncertainties associated with luminance non-uniformity and non-Lambertian emission patterns in the efficiency characterizations.

Ideally, achieving uniform distribution of luminance should be an important prerequisite for characterizing and reporting the CE or luminance of QLEDs. In practice, as we discussed above, the QLEDs fabricated in the research labs can exhibit non-uniform luminance across the active area. If the operational stabilities of these non-ideal devices have to be characterized, we highlight that special attention should be paid to the determination of the initial *average* luminance, instead of the initial luminance from a given small area. Supplementary Fig. 7 shows an example of the lifetime measurement on a QLED with luminance concentrated in the central region of the device. The luminance-decay curves with the initial luminance determined by using a luminance meter (red curve) that detects the *local* luminance (red circle, Supplementary Fig. 7a), or determined by using an integrating-sphere photometer

(blue curve) that detects the *average* luminance (blue square, Supplementary Fig. 7a) are shown in Supplementary Fig. 7b. The use of a luminance meter measuring the *local* luminance caused a two-fold overestimation of the initial *average* luminance. As a result, the extrapolated T_{50} lifetime at an initial luminance of 100 cd m^{-2} is overestimated by ~5 folds (acceleration factor assumed to be 1.9). Furthermore, the QLEDs with non-uniform luminance could show pronounced changes in the luminance distributions (or in the luminous area) during the long-term operation. An example is shown in Supplementary Fig. 8. The spatial evolution of luminance may not be resolved in the operation-lifetime measurements, which commonly employ a photodetector with a large acceptance angle to monitor the *average* luminance of the whole device area. Therefore, defining the initial luminance of the QLEDs by their initial *average* luminance is a more appropriate and consistent approach in daily lifetime measurements.

Overall, we suggest that the luminance uniformity of the QLEDs should be examined and the initial luminance should be accurately determined before the lifetime measurements. Integrating-sphere photometer or goniometric photometer are preferred methods to measure the initial *average* luminance of the QLED. To gain further insights into the degradation processes of the QLEDs with non-uniform luminance, spatial-resolved characterizations on the distributions and evolutions of both luminance and current density are demanded.

Analysis of luminance-decay curves

It has been widely observed that in lifetime measurements of QLEDs, the evolution of luminance could exhibit distinctive features, adding to another dimension of complexity in the extraction of operational lifetimes. Figure 6a shows two typical luminance decay curves measured from the blue QLEDs fabricated in our lab. The red curve shows the stretched-exponential decay characteristics. The blue curve shows a 'stabilization period' (or 'burn-in period') featuring a rapid decrease in luminance. The time required for stabilization (T_S), which may vary depending on the material properties and driving currents, ranges from minutes to hours. Borrowed from the experience of lifetime assessment of organic LEDs and perovskite LEDs or photovoltaic devices[48–51], the stabilization periods of QLEDs may not be directly related to the intrinsic degradation processes. This is supported by the plot of $\log[\ln(L_0/L_t)]$ versus $\log(t)$ for the two luminance-decay curves (Fig. 6b). While the stretched-exponential luminance decay manifests as a linear relation of $\log[\ln(L_0/L_t)]-\log(t)$ (red squares) as predicted by Eqs. (14) and (15), the luminance-decay curve with stabilization periods show deviations from the linear relation in the $\log[\ln(L_0/L_t)]-\log(t)$ plot (blue solid circles). Future efforts are needed to elucidate the mechanism accounting for the stabilization period. At this stage, for the determination of operation lifetime that enables valid comparisons between different QLEDs, we suggest that T_S should be excluded in the analysis so that the operational lifetime corresponding to the intrinsic degradation can be extracted from the luminance decay starting from a stabilized initial luminance (L_S, Fig. 6a). After excluding the stabilization periods, the luminance-decay curves now show linear relations in the $\log[\ln(L_S/L_t)]-\log(t)$ plot (blue hollow circles, Fig. 6b), indicating the ideal stretched exponential decay characteristics induced by intrinsic degradations of the QLEDs.

Besides, it is often observed that in operational-lifetime measurements, the luminance could show an initial ramp (Supplementary Fig. 9). The luminance-ramp period could last for tens or even hundreds of hours, depending on the materials and device structure of the QLEDs. In these cases, we suggest researchers present a complete curve of the luminance evolution and make a clear statement on how the initial luminance and the corresponding operational lifetime are defined. We note that from
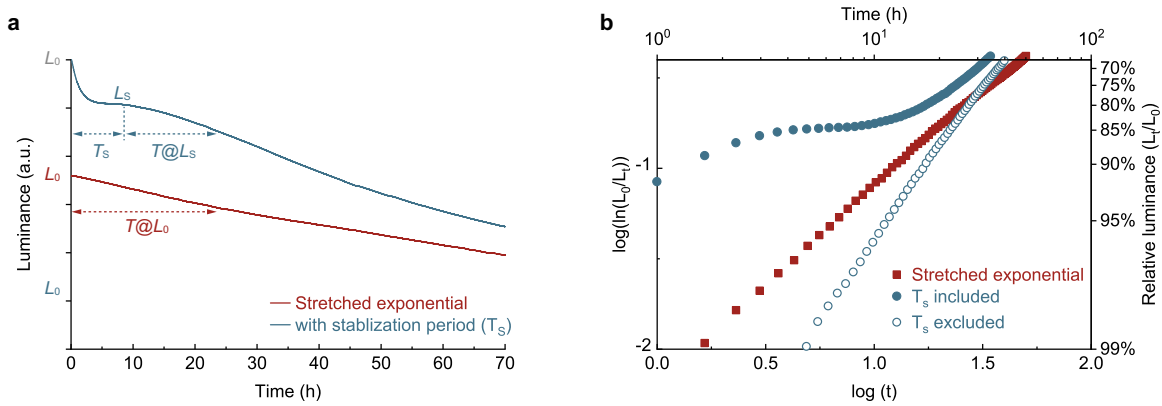
Fig. 6 Extraction of lifetime in operational-lifetime measurements. a Two typical shapes of the luminance-decay curves of QLEDs, i.e., stretched-exponential decay (red curve), and a rapid decrease followed by a slow decrease (blue curve) in the luminance. For the latter situation, we recommend that the lifetime should be extracted from the luminance decrease with respect to a stabilized luminance ($T@L_s$), with the stabilization period (T_s) excluded. **b** Plots of $\log[\ln(L_0/L_t)]$ versus $\log(t)$ for the stretched-exponential luminance-decay curve (red squares, linear) and the luminance-decay curve with stabilization period (blue solid circles, non-linear). The blue hollow circles correspond to the luminance-decay curve with T_s excluded, indicating a linear relation of $\log[\ln(L_0/L_t)]-\log(t)$.

a technical perspective, the initial luminance ramp of the QLEDs can potentially be counted after developing advanced compensation methods together with matched driving circuits in real display panels. Thus, the stabilization periods may be useful in the future development of active-matrix QLED panels. Currently, presenting the complete luminance-time curve in the report of operation lifetime may enable comprehensive assessments of the device stability.

Protocols and checklist
Our discussions highlight the critical importance of appropriate choices of characterization methods, rigorous calibrations of the instruments, and unified methods of data analysis. To accomplish the above considerations, we suggest a set of testing protocols for the efficiency and lifetime measurements of QLEDs (Supplementary Table 3). Besides, a checklist is provided alongside the protocols, in which the researchers are encouraged to record the necessary information about the experimental environment, instrumental specifications, measurement parameters (e.g., integration time for the detector, and the delay time in the voltage-sweep measurement), and device characteristics (see Supplementary Table 3 for details). Having all the critical considerations addressed, one should note that there could still exist relative errors of 1–5% in the measured quantities, which originate from the uncertainties in the light output of the standard lamps used for calibrations. Besides the report of device parameters, examples of the graphic demonstration of device characteristics are demonstrated in Supplementary Fig. 10.

In summary, we have demonstrated that the accuracy of QLED characterizations can be affected by the non-ideal EL properties of the device and the data processing procedures in the measurements. In the efficiency characterizations, considerable errors and uncertainties could arise from the non-uniform luminance across the active area and the non-Lambertian angular distribution of EL intensities. Besides, the inconsistent use of the luminous efficiency functions could cause systematical errors in the radiometric-to-photometric conversions in the efficiency measurements. Furthermore, we suggest that the determination of operational lifetime is largely affected by the accuracy of the initial luminance and the analyses of the luminance-decay curves. Therefore, appropriate choice of characterization methods, rigorous calibration of the testing system, use of standard luminous efficiency function, and full report of the measurement details and parameters are required to reduce the errors and ambiguities in the measurements of device

metrics. A set of measurement protocols and a checklist are proposed to promote the reliable and consistent characterizations of QLEDs, which shall provide a basis for valid comparisons between different devices. We expect that the findings reported in this work may help researchers in the QLED field develop the best measurement practice, ultimately leading to the more rapid progress of QLED technology towards display applications.

METHODS
Materials
Poly(3,4-ethylenedioxythiophene)-poly(styrenesulfonate) (PEDOT:PSS, Clevious PVP AI 4083) was purchased from Heraeus. Poly[(9,9-dioctyl-fluorenyl-2,7-diyl)-alt-(4,4'-(N-(4-butylphenyl)))] (TFB) was purchased from American Dye Source. Chlorobenzene (99.8%, ultra-dry), n-octane (99%, ultra-dry), and ethanol (99.5%, ultra-dry) were purchased from Acros. The materials for thermal evaporation were purchased from ZhongNuo Advanced Material (Beijing) Technology Co., Ltd. The red CdSe/CdZnSe/ZnS core/shell/shell QDs, green CdSe/CdZnSe/ZnS core/shell/shell QDs and blue CdZnSe/ZnS core/shell QDs used for the bottom-emitting QLEDs were provided by Najing Technology. The red CdZnSe/ZnS core/shell QDs, green CdZnSeS/ZnS QDs and blue CdZnSeS/ZnS QDs used for the top-emitting QLEDs were purchased from Suzhou Xingshuo Nanotech Co., Ltd. The $Zn_{0.9}Mg_{0.1}O$ nanoparticles were synthesized according to a previous report[52].

Fabrication of bottom-emitting QLEDs
The device structure of the QLEDs is ITO/PEDOT:PSS/TFB/QDs/$Zn_{0.1}Mg_{0.9}O$/cathode. PEDOT:PSS solutions were spin-coated on the cleaned ITO-coated glass substrates (sheet resistance: $20\,\Omega\,sq^{-1}$) at 3000 r.p.m. for 45 s.The PEDOT:PSS-coated substrates were annealed at 150 °C for 30 min. Then, the substrates were transferred into a glovebox filled with nitrogen. Chlorobenzene solutions of TFB ($12\,mg\,mL^{-1}$) were spin-coated at 2000 r.p.m. for 40 s and baked at 150 °C for 30 min. Then, the red or blue QDs (in octane, $20\,mg\,mL^{-1}$) and $Zn_{0.9}Mg_{0.1}O$ particles (in ethanol, 30–90 mg mL^{-1}) were sequentially deposited by spin-coating at 2000 r.p.m. for 40 s and 3000 r.p.m. for 30 s, respectively. Finally, the aluminum electrode with a thickness of 100 nm was deposited in the thermal evaporation system (Trovato 300C). The devices were encapsulated by covering glasses using ultraviolet curable resin (Loctite AA3492). To prepare the QLEDs with non-uniform luminance, silver electrode was employed as the cathode and the devices were stored for several weeks.

Fabrication of top-emitting QLEDs
The top-emitting QLED possesses a structure of glass/Ag/IZO/PEDOT:PSS/TFB/red-QDs: green-QDs: blue-QDs (blending ratio 1:12:39)/ZnMgO /Al/IZO. Briefly, the Ag and IZO layers with a thickness of 100 and 60 nm,

respectively, were deposited onto glass substrates by a magnetron sputtering system at a working pressure of 0.45 Pa, a power of 50 W and an Ar flow of 20 sccm. Then, the samples were treated with O_2 plasma for 5 min. The PEDOT:PSS, TFB, QDs and ZnMgO nanoparticles were deposited in sequence by using similar spin-coating parameters as for bottom-emitting QLEDs. Afterwards, the samples were transferred to a high-vacuum evaporation chamber to deposit a 2 nm Al as a sputtering protective layer at a base pressure of 5×10^{-4} Pa (deposition rate: 1–2 Å/s). Finally, the samples were transferred to a magnetron sputtering system to deposit a IZO layers with a thickness of 80 nm at a working pressure of 0.45 Pa, a power of 50 W and an Ar flow of 20 sccm.

Characterization of luminance uniformity
The microscopy images of the luminous area of the operating QLEDs were acquired by using an inverted routine microscope (Axio Vert.A1, Zeiss) coupled with a camera (Axiocam MRc 5, Zeiss). The devices were biased stressed before the characterizations. The integration time is automatically set to avoid overexposure. The brightness histograms were obtained from the images converted to gray scales. The relative standard deviations of the brightness distributions (RSD_L) were determined according to the equation of:

$$RSD_L = SD_L/A_L = \sqrt{\frac{\sum_{i=1}^{n} (L_i - A_L)^2}{n-1}}/A_L \tag{19}$$

where L_i, SD_L, and A_L represent the brightness of a pixel in the luminous area, the standards deviation and the average value of the brightness, respectively.

Characterization of QLEDs using a luminance meter
The luminance, EL spectra, current density, and voltage of the QLEDs were simultaneously characterized by using a commercial luminance meter (SRC-600, Everfine). The devices were fixed on a precise 2D translation stage with the luminous surface perpendicular to the detector. The device-to-detector distance was 350 mm. The measurement field angle of the detection system was set as 0.1° or 0.2°. The detection position was changed by adjusting the translation stage. Each measurement was performed after applying electrical stress (constant current density) on the device for 15 s to reach a stable state.

Characterization of QLEDs using an integrating-sphere photometer
The current density–voltage characteristics of the QLEDs were measured by a source meter (Keithley 2400, Tektronix). The EL characteristics of devices were measured by using a customized integrating-sphere photometer (Labsphere) coupled with a CCD spectrometer (QE Pro, Ocean Optics). The system was calibrated with a standard lamp (HL-3 plus, Ocean Optics) with reference spectral radiant flux. Detailed information on the design and calibration of the integrating-sphere photometer is shown in Supplementary Fig. 1. The entrance aperture (diameter: 9.5 mm) is larger than the luminous area of the device (2×2 mm^2) and smaller than the glass substrates (19×19 mm^2). The device region of the glass substrates is in contact with the entrance aperture of the integrating sphere. Thus, all the photos emitting into the forward hemisphere can be collected by the integrating sphere while the edge-emitted photons were excluded.

Characterization of QLEDs using a goniometric photometer
The intensity distribution of QLEDs was obtained by using a home-built goniometric photometer with a photodetector (PDA100A2, Thorlabs) rotating around the QLEDs. The sample-to-detector distance was 150 mm and the acceptance angle of the detector at a given viewing angle was ~4°. The viewing angle of the photodetector was varied from 0° to 80° with a step of 5° or 10°. The QLED was driven by a source meter (Keithley 2400) at a constant current density corresponding to a luminance of 2000 cd m^{-2}. The edge of glass substrates was covered by black tape to prevent the edge-emitted light from entering the detector.

Optical simulation of emission pattern of QLEDs
The angular distribution of the intensities of QLEDs was simulated based on the electrical-dipole model according to the previous reports[53,54]. Briefly, the spontaneous emission of QDs in a microcavity consisting of multiple layers was described as a weighted sum of radiation from three orthogonally oriented dipoles. The reflection, interference, and near-field interactions with

the metal electrodes were taken into consideration. The total radiation power density, as well as the power density transmitted into air (K_{air}), were calculated as a function of the in-plane wavevector (k_p). The power density distribution as a function of the viewing angle (θ_{air}) was determined according to:

$$P(\theta_{air}) = \frac{k_e^2 \cos(\theta_{air})}{\pi} K_{air}(k_p) \tag{20}$$

where k_e is the wavenumber in the emissive layer.

DATA AVAILABILITY
The data that support the finding of this study are available from the corresponding authors upon reasonable request.

REFERENCES
1. Colvin, V. L., Schlamp, M. C. & Alivisatos, A. P. Light-emitting-diodes made from cadmium selenide nanocrystals and a semiconducting polymer. *Nature* **370**, 354–357 (1994).
2. Coe, S., Woo, W. K., Bawendi, M. & Bulović, V. Electroluminescence from single monolayers of nanocrystals in molecular organic devices. *Nature* **420**, 800–803 (2002).
3. Sun, Q. et al. Bright, multicoloured light-emitting diodes based on quantum dots. *Nat. Photonics* **1**, 717–722 (2007).
4. Caruge, J. M., Halpert, J. E., Wood, V., Bulovic, V. & Bawendi, M. G. Colloidal quantum-dot light-emitting diodes with metal-oxide charge transport layers. *Nat. Photonics* **2**, 247–250 (2008).
5. Qian, L., Zheng, Y., Xue, J. & Holloway, P. H. Stable and efficient quantum-dot light-emitting diodes based on solution-processed multilayer structures. *Nat. Photonics* **5**, 543–548 (2011).
6. Mashford, B. S. et al. High-efficiency quantum-dot light-emitting devices with enhanced charge injection. *Nat. Photonics* **7**, 407–412 (2013).
7. Kwak, J. et al. Bright and efficient full-color colloidal quantum dot light-emitting diodes using an inverted device structure. *Nano Lett.* **12**, 2362–2366 (2012).
8. Alivisatos, A. P. Semiconductor clusters, nanocrystals, and quantum dots. *Science* **271**, 933–937 (1996).
9. Kagan, C. R., Lifshitz, E., Sargent, E. H. & Talapin, D. V. Building devices from colloidal quantum dots. *Science* **353**, aac5523 (2016).
10. Pu, C. et al. Synthetic control of exciton behavior in colloidal quantum dots. *J. Am. Chem. Soc.* **139**, 3302–3311 (2017).
11. Arquer, F. P. Gd et al. Semiconductor quantum dots: technological progress and future challenges. *Science* **373**, eaaz8541 (2021).
12. Shirasaki, Y., Supran, G. J., Bawendi, M. G. & Bulovic, V. Emergence of colloidal quantum-dot light-emitting technologies. *Nat. Photonics* **7**, 13–23 (2013).
13. Dai, X., Deng, Y., Peng, X. & Jin, Y. Quantum-dot light-emitting diodes for large-area displays: towards the dawn of commercialization. *Adv. Mater.* **29**, 22 (2017).
14. Liu, M. et al. Colloidal quantum dot electronics. *Nat. Electron.* **4**, 548–558 (2021).
15. Dai, X. et al. Solution-processed, high-performance light-emitting diodes based on quantum dots. *Nature* **515**, 96–99 (2014).
16. Yang, Y. et al. High-efficiency light-emitting devices based on quantum dots with tailored nanostructures. *Nat. Photonics* **9**, 259–266 (2015).
17. Cao, W. et al. Highly stable QLEDs with improved hole injection via quantum dot structure tailoring. *Nat. Commun.* **9**, 2608 (2018).
18. Lim, J., Park, Y.-S., Wu, K., Yun, H. J. & Klimov, V. I. Droop-free colloidal quantum dot light-emitting diodes. *Nano Lett.* **18**, 6645–6653 (2018).
19. Shen, H. et al. Visible quantum dot light-emitting diodes with simultaneous high brightness and efficiency. *Nat. Photonics* **13**, 192–197 (2019).
20. Won, Y.-H. et al. Highly efficient and stable InP/ZnSe/ZnS quantum dot light-emitting diodes. *Nature* **575**, 634–638 (2019).
21. Pu, C. et al. Electrochemically-stable ligands bridge the photoluminescence-electroluminescence gap of quantum dots. *Nat. Commun.* **11**, 937 (2020).
22. Li, X. et al. Quantum-dot light-emitting diodes for outdoor displays with high stability at high brightness. *Adv. Opt. Mater.* **8**, 1901145 (2020).
23. Liu, D. et al. Highly stable red quantum dot light-emitting diodes with long T_{95} operation lifetimes. *J. Phys. Chem. Lett.* **11**, 3111–3115 (2020).
24. Kim, T. et al. Efficient and stable blue quantum dot light-emitting diode. *Nature* **586**, 385–389 (2020).
25. Chen, D. et al. Shelf-stable quantum-dot light-emitting diodes with high operational performance. *Adv. Mater.* **32**, 2006178 (2020).
26. Lee, T. et al. Bright and stable quantum dot light-emitting diodes. *Adv. Mater.* **34**, 2106276 (2021).

27. Jeong, S. -H. et al. Characterizing the efficiency of perovskite solar cells and light-emitting diodes. *Joule* **4**, 1206–1235 (2020).

28. Anaya, M. et al. Best practices for measuring emerging light-emitting diode technologies. *Nat. Photonics* **13**, 818–821 (2019).

29. Forrest, S. R., Bradley, D. D. C. & Thompson, M. E. Measuring the efficiency of organic light-emitting devices. *Adv. Mater.* **15**, 1043–1048 (2003).

30. Schubert, E. F. *Light-Emitting Diodes* (Cambridge University Press, 2003).

31. Tsutsui, T. & Takada, N. Progress in emission efficiency of organic light-emitting diodes: basic understanding and its technical application. *Jpn. J. Appl. Phys.* **52**, 110001 (2013).

32. International Commission on Illumination. *Test Method for LED Lamps, LED Luminaires and LED Modules* (CIE S 025/E:2015) (International Commission on Illumination, 2015).

33. Illuminating Engineering Society. *Approved Method Electrical and Photometric Measurements of Solid-State Lighting Products* (IES LM-79-08). (Illuminating Engineering Society, New York, USA, 2008).

34. Illuminating Engineering Society. *Approved Method Total Flux Measurement of Lamps Using an Integrating Sphere* (IES LM-78-17) (Illuminating Engineering Society, 2017).

35. Scholz, S., Kondakov, D., Lüssem, B. & Leo, K. Degradation mechanisms and reactions in organic light-emitting devices. *Chem. Rev.* **115**, 8449–8503 (2015).

36. Féry, C., Racine, B., Vaufrey, D., Doyeux, H. & Cinà, S. Physical mechanism responsible for the stretched exponential decay behavior of aging organic light-emitting diodes. *Appl. Phys. Lett.* **87**, 213502 (2005).

37. International Electrotechnical Commission. *Organic Light Emitting Diode (Oled) Displays—Part 5-3: Measuring Methods of Image Sticking and Lifetime* (IEC 62341-5-3) (International Electrotechnical Commission, 2013).

38. Acharya, K. P. et al. High efficiency quantum dot light emitting diodes from positive aging. *Nanoscale* **9**, 14451–14457 (2017).

39. Su, Q., Sun, Y., Zhang, H. & Chen, S. Origin of positive aging in quantum-dot light-emitting diodes. *Adv. Sci.* **5**, 1870058 (2018).

40. Kim, J.-S., Ho, P. K., Greenham, N. C. & Friend, R. H. Electroluminescence emission pattern of organic light-emitting diodes: Implications for device efficiency calculations. *J. Appl. Phys.* **88**, 1073–1081 (2000).

41. International Commission on Illumination. *Colorimetry-Part 1: CIE Standard Colomertric Observers* (ISO/CIE 11664-1:2019). (International Commission on Illumination, 2019).

42. Ohno, Y. et al. Principles governing photometry (2nd edition). *Metrologia* **57**, 020401 (2020).

43. Vos, J. J. Colorimetric and photometric properties of a 2° fundamental observer. *Color Res. Appl.* **3**, 125–128 (1978).

44. International Commission on Illumination. *CIE 1988 2° Spectral Luminous Efficiency Function for Photopic Vision* (CIE 86-1990) (International Commission on Illumination, 1990).

45. Stockman, A. Cone fundamentals and CIE standards. *Curr. Opin. Behav. Sci.* **30**, 87–93 (2019).

46. Sharpe, L. T., Stockman, A., Jagla, W. & Jägle, H. A luminous efficiency function, $V^*(\lambda)$, for daylight adaptation. *J. Vis.* **5**, 948–968 (2005).

47. International Commission on Illumination. *Fundamental Chromaticity Disagram with Physiological Axes-Part 2: Spectral Luminous Efficiency Functions and Chromaticity Diagrams* (CIE 170:2-2015) (International Commission on Illumination, 2015).

48. Reese, M. O. et al. Consensus stability testing protocols for organic photovoltaic materials and devices. *Sol. Energy Mater. Sol. Cells* **95**, 1253–1267 (2011).

49. Khenkin, M. V. et al. Consensus statement for stability assessment and reporting for perovskite photovoltaics based on ISOS procedures. *Nat. Energy* **5**, 35–49 (2020).

50. Liu, X.-K. et al. Metal halide perovskites for light-emitting diodes. *Nat. Mater.* **20**, 10–21 (2021).

51. Parker, I. D., Cao, Y. & Yang, C. Y. Lifetime and degradation effects in polymer light-emitting diodes. *J. Appl. Phys.* **85**, 2441–2447 (1999).

52. Zhang, Z. et al. High-performance, solution-processed, and insulating-layer-free light-emitting diodes based on colloidal quantum dots. *Adv. Mater.* **30**, 1801387 (2018).

53. Furno, M., Meerheim, R., Hofmann, S., Lüssem, B. & Leo, K. Efficiency and rate of spontaneous emission in organic electroluminescent devices. *Phys. Rev. B* **85**, 115205 (2012).

54. Cui, J. et al. Efficient light-emitting diodes based on oriented perovskite nano-platelets. *Sci. Adv.* **7**, eabg8458 (2021).

ACKNOWLEDGEMENTS

AUTHOR CONTRIBUTIONS
Y.J. and Y.D. conceived the idea and designed the experiments. Y.J. supervised the work and finalized the manuscript. W.J. fabricated the QLEDs, carried out the efficiency measurements, microscopic measurements, and analyzed the results. Y.D. performed optical simulations on the QLEDs, carried out the operational-lifetime measurements, and assisted in analyzing the results. B.G., Y.L., B.Z., and D.D. assisted in the measurements using luminance meter. Y.D. and Y.J. wrote the first draft of the manuscript. All authors discussed the results and commented on the manuscript.

COMPETING INTERESTS
The authors declare no competing interests.

ADDITIONAL INFORMATION
Supplementary information The online version contains supplementary material available at https://doi.org/10.1038/s41528-022-00169-5.

Correspondence and requests for materials should be addressed to Yunzhou Deng or Yizheng Jin.

Reprints and permission information is available at http://www.nature.com/reprints

Publisher's note Springer Nature remains neutral with regard to jurisdictional claims in published maps and institutional affiliations.